Ann. Geophys., 25, 1417–1432, 2007
www.ann-geophys.net/25/1417/2007/

Annales Geophysicae

Temperature anisotropies of electrons and two-component protons in the dusk plasma sheet

M. N. Nishino[1], M. Fujimoto[1], T. Terasawa[2], G. Ueno[3], K. Maezawa[1], T. Mukai[4], and Y. Saito[1]

[1]ISAS/JAXA, Kanagawa 229-8510, Japan
[2]Tokyo Institute of Technology, Tokyo 152-8551, Japan
[3]Institute of Statistical Mathematics, Tokyo 106-8569, Japan
[4]JAXA, Tokyo 100-8260, Japan

Received: 3 April 2007 – Revised: 12 June 2007 – Accepted: 18 June 2007 – Published: 29 June 2007

Abstract. To investigate the cold plasma sheet formation under northward IMF, we study the temperature anisotropies of electrons and two-component protons observed by the Geotail spacecraft. The two-component protons, which are occasionally observed in the dusk plasma sheet near the low-latitude boundary, are the result of spatial mixing of the hot protons of the magnetosphere proper and the cold protons from the solar wind. Recent research focusing on the two-component protons reported that the cold proton component at times has a strong anisotropy, and that the sense of the anisotropy depends on the observed locations. Since electrons have been known to possess a strong parallel anisotropy around the low-latitude boundary layer, we compare anisotropies of electrons and protons to find that the strengths of parallel anisotropies of electrons and the cold proton component are in good correlation in the tail flank. The parallel anisotropy of electrons is stronger than that of the cold proton component, which is attributed to selective heating of electrons. We further find that the strengths of the parallel anisotropies in the tail flank depend on the latitudinal angle of the IMF; strong parallel anisotropies occur under strongly northward IMF. We discuss that the Kelvin-Helmholtz vortices, which developed under strongly northward IMF, and the resultant magnetic reconnection therein may lead to the strong parallel anisotropies observed in the tail flank.

Keywords. Magnetospheric physics (Magnetotail; Magnetotail boundary layers; Plasma sheet)

1 Introduction

The near-Earth plasma sheet has been known to become cold and dense when the interplanetary magnetic field (IMF) points northward (e.g. Zwolakowska et al., 1992; Zwolakowska and Popielawska, 1992; Terasawa et al., 1997; Borovsky et al., 1998; Nishino et al., 2002; Wing et al., 2005). Since the trend of low temperature is more typical in the dawn and dusk flank regions than in the midnight region, the cold plasma is thought to be of the solar wind origin and to come through the flanks (Terasawa et al., 1997). However, the entry process of solar wind plasma into the plasma sheet under northward IMF has not been totally understood. Signatures of the cold plasma sheet may provide some clue to understanding the solar wind entry and resultant formation of the cold plasma sheet.

An interesting feature of the cold plasma sheet is the occasional coexistence of cold and hot protons near the magnetopause (Eastman et al., 1976; Sckopke et al., 1981). In particular, recent satellite observations have revealed that two separate components of cold and hot protons coexist in the dusk plasma sheet under northward IMF (Fujimoto et al., 1998; Hasegawa et al., 2003; Nishino et al., 2005; Wing et al., 2005). These two components of protons are thought to have separate origins: the cold component from the solar wind and the hot component of magnetospheric origin. To study signatures of the cold plasma sheet with the two-component protons is important to understand the formation of the cold plasma sheet under northward IMF.

It has been reported that electrons and protons in the Earth's magnetosphere have significant temperature anisotropies, which are regarded as a useful tool in diagnosing the physical processes that the plasma undergo there. As for protons, it has been widely accepted that protons in the near-Earth plasma sheet are roughly isotropic or possess a perpendicular anisotropy with the perpendicular temperature exceeding the parallel temperature (Mauk and McPherron, 1980). Concerning the cold protons, Traver et al. (1991) reported that the protons in the plasma sheet near the low-latitude boundary possess a parallel anisotropy under northward IMF. On the other hand, Wing et al. (2005) pointed out

Correspondence to: M. N. Nishino
(nishino@stp.isas.jaxa.jp)

Published by Copernicus Publications on behalf of the European Geosciences Union.

a perpendicular anisotropy of the cold protons in the dayside plasma sheet near the low-latitude boundary. Recently, Nishino et al. (2007), analyzing the temperature anisotropy of two-component protons in the dusk plasma sheet near the low-latitude boundary, found that the cold proton component occasionally possesses a strong anisotropy, and that the sense of the anisotropy depends on the observed locations; parallel temperature is enhanced in the tail flank, while perpendicular temperature is enhanced on the dayside. They have also reported that the hot proton component is nearly isotropic in the tail while the perpendicular temperature is enhanced on the dayside, which is roughly consistent with the statistical picture of the plasma sheet (Mauk and McPherron, 1980).

In addition to protons, it has also been known that electrons at times possess a temperature anisotropy around the magnetopause. In the flank plasma sheet and the low-latitude boundary layer (LLBL), a parallel anisotropy of electrons has been observed under northward IMF (or geomagnetically quiet condition) (Hada et al., 1981; Traver et al., 1991; Phan et al., 1997; Fujimoto et al., 1998; Gary et al., 2005). In particular, a strong parallel anisotropy is observed in the Earth-side region in the LLBL, where the parallel electron temperature is about 3 times as high as the perpendicular electron temperature (Phan et al., 1997). In contrast, a perpendicular anisotropy of electrons is observed in the plasma depletion layer that forms in front of the dayside magnetopause under northward IMF (Phan et al., 1996). Therefore, the parallel anisotropy of electrons in the LLBL should be attributed to some physical process(es) within the magnetosphere.

Adiabatic change in the magnetotail is a candidate for plasma heating and resultant temperature anisotropies (e.g. Treumann and Baumjohann, 1997). Owing to conservations of the first and second adiabatic invariants, both electrons and protons undergo heating in both perpendicular and parallel directions, as a result of the interplay between betatron and Fermi accelerations, as they move earthward in the plasma sheet (e.g. Cowley and Ashour-Abdalla, 1975; Yamamoto and Tamao, 1978). A parallel anisotropy of electrons in the plasma sheet was shown by observational studies (Hada et al., 1981; Sugiyama et al., 1997; Shiokawa et al., 2003) in which the possibility of Fermi acceleration of electrons in the plasma sheet was discussed. A recent study by Nishino et al. (2007) suggested that some portion of the observed parallel anisotropy of the cold proton component in the dusk flank plasma sheet could be explained by adiabatic heating.

Although both electron and proton anisotropies have been known to exist in the cold plasma sheet, they have been discussed separately in past studies and their relation has not been examined yet. In this paper, we study temperature anisotropies of electrons and two-component protons in the plasma sheet near the dusk low-latitude boundary.

2 Instrumentation

We use data from three-dimensional (3-D) ion and electron distribution functions obtained every 12 s by the low energy particle (Geotail/LEP) experiment (Mukai et al., 1994) and the magnetic field data obtained by the flux-gate magnetometer (Geotail/MGF) (Kokubun et al., 1994). The ion energy-per-charge analyzer of LEP-EAi detects ions between 32 eV/q and 39 keV/q, which covers most of the typical energy range of plasma sheet protons. The electrons are detected by the electron analyzer of LEP-EAe, which is operated with the two energy ranges; one is from 60 eV to 38 keV (high-energy mode) and the other is from 8.3 eV to 7.6 keV (low-energy mode). Solar wind parameters obtained by the Wind and the ACE spacecraft were provided by CDAWeb. The Wind data are from SWE (Ogilvie et al., 1995) and MFI (Lepping et al., 1995), and the ACE data are from MFI (Smith et al., 1998) and SWEPAM (McComas et al., 1998).

3 Calculation of moment parameters

In order to separate the ion distribution function into cold and hot components, we utilize a two-Maxwellian mixture model with a scheme developed by Ueno et al. (2001a). In this scheme we use the ion phase space density (PSD) to estimate densities, velocities and pressure tensors of the cold and hot components with an algorithm based on maximum likelihood, assuming that all of the detected positive ions are protons. Perpendicular and parallel temperatures of the cold and hot components are calculated from the pressure tensors. We denote these temperatures as $T_{C\perp}$, $T_{C\parallel}$, $T_{H\perp}$, and $T_{H\parallel}$, respectively.

As for electrons, we perform simple moment calculations to obtain effective perpendicular and parallel temperatures, which are denoted as $T_{e\perp}$, $T_{e\parallel}$, respectively. For the interval of the low-energy mode, we utilize electron PSD with energy higher than 12.86 eV, in order to exclude the effects of photoelectrons whose energy is typically lower than 10 eV in and around the cold plasma sheet of our interest (Ishisaka et al., 2001). Since some of the detected photoelectrons have kinetic energy higher than the electric potential of the satellite (Ueno et al., 2001b), the lower limit is set to be higher than the satellite potential.

4 Case studies

4.1 24 March 1995 event (dusk tail-flank)

On 24 March 1995, protons in the dusk plasma sheet near the low-latitude boundary consisted of two separate components, and the cold proton component possessed a strong parallel anisotropy. We first revisit this event to investigate anisotropies of both electrons and protons.

The IMF pointed strongly northward between 00:00–08:00 UT, and it kept the northward polarity after 08:00 UT (see Nishino et al., 2007, for details). The maximum latitudinal angle of the IMF in the 1-h averaged data was as large as 84 degrees (between 02:00–03:00 UT at the Wind location). The solar wind density was higher than 10 cm^{-3} throughout the interval, and its speed was as slow as about 330–340 km/s (∼0.6 keV). The convection time of the solar wind from the Wind location ($X \sim 219\ R_E$) to the Earth's magnetosphere was about 70 min.

On this day Geotail came from the dusk magnetosheath into the magnetosphere and observed the cold plasma sheet in the midst of the prolonged northward IMF interval (Fujimoto et al., 1998; Fairfield et al., 2000). Figure 1 shows (a) ion and (b) electron data between 09:00–10:00 UT observed by Geotail. In panel (a), from the top, E-t spectrograms of omni-directional, sunward, and tailward ions, temperatures and densities of cold and hot proton components are presented. The perpendicular (parallel) temperature is shown by the green (blue) points, and the density of the cold (hot) component is shown by the blue (red) points. Panel (b) shows the electron observations; E-t spectrogram of omni-directional electrons and temperatures are shown. Until 09:10 UT Geotail was in the LLBL with dense tailward flows ($V_X \sim -100$ km/s), and after 09:11 UT it was in the stagnant cold plasma sheet (Fairfield et al., 2000). At 09:10 UT Geotail was located at (−15.3, 18.4, 2.2) R_E in the GSM coordinates. We focus on the interval between 09:11–09:59 UT when two peaks of the ion counts in the energy space are evident (Nishino et al., 2007).

As was studied by Nishino et al. (2007), throughout the interval after 09:11 UT, the cold proton component has a strong parallel anisotropy, $T_{C\perp}/T_{C\parallel} \sim 0.47$, where $T_{C\perp}$ and $T_{C\parallel}$ were about 100 eV and 210 eV, respectively. Anisotropy of the hot component was much weaker than that of the cold component, with the perpendicular and parallel temperatures ($T_{H\perp}$ and $T_{H\parallel}$) being 1.9 keV and 2.2 keV, which give $T_{H\perp}/T_{H\parallel} \sim 0.87$. As for densities of the two components, the cold component (2.2 cm^{-3}) dominated over the hot component (0.3 cm^{-3}). However, thermal pressures of the hot component in the perpendicular and parallel directions (83 pPa and 97 pPa) were comparable to or still higher than those of the cold component (36 pPa and 75 pPa).

Next we study signatures of electrons in the plasma sheet. Since the LEP-EAe was operated in the low-energy mode (from 8.3 eV to 7.6 keV) throughout the interval of our interest, original electron PSD data includes a high contribution of the photoelectrons which are seen in the lower energy range (<10 eV) of the electron E-t spectrogram. The effect of the photoelectrons is eliminated in the following moment calculations. For the interval of our interest, the electron in the plasma sheet had a strong parallel anisotropy. The averaged electron anisotropy ($T_{e\perp}/T_{e\parallel}$) was 0.37, where $T_{e\perp}$ and $T_{e\parallel}$ were 32 eV and 86 eV, respectively. The parallel anisotropy of electrons was stronger than that of the cold proton component ($T_{C\perp}/T_{C\parallel} \sim 0.47$). The ratio of the cold-proton temperature to the electron temperature is roughly as low as 3, which is much lower than the typical ratio that is as high as 7 (Baumjohann, 1993).

Figures 2a and b show two-dimensional (2-D) cuts of the ion and electron PSDs for the 12-s interval between 09:30:10–09:30:22 UT in the plane that includes the magnetic field that was (11.9, −7.5, 8.9) nT in the GSM coordinates, whose direction is shown by a red arrow in the figure. The left (right) portion of each cut shows the sunward (tailward) moving particles, and the maximum speeds shown in the figure are about 2100 km/s for ions and 23 900 km/s for electrons, respectively. The temperature anisotropies for the interval were $T_{C\perp}/T_{C\parallel} \sim 0.41$, $T_{H\perp}/T_{H\parallel} \sim 0.79$, and $T_{e\perp}/T_{e\parallel} \sim 0.40$, where $T_{C\perp} \sim 99$ eV, $T_{C\parallel} \sim 240$ eV, $T_{H\perp} \sim 1.9$ keV, $T_{H\parallel} \sim 2.4$ keV, $T_{e\perp} \sim 35$ eV, and $T_{e\parallel} \sim 88$ eV, respectively. Elongations of the PSD contours (yellow-red colored region in Figs. 2a and b) in the direction parallel to the magnetic field are owing to the strong parallel anisotropies of the cold proton component and the electrons.

Figures 2c and d show one-dimensional (1-D) cuts of ion and electron PSDs in the direction parallel and perpendicular to the local magnetic field. Green (blue) lines correspond to the PSDs in the perpendicular (parallel) direction, and the pink lines correspond to the one-count level. The ions consist of the cold and hot components, and the electrons are a superposition of the photoelectron component and the ambient electron component. A couple of vertical red broken lines in Fig. 2d correspond to the lowest energy used for the temperature calculations. We find that the low-energy part of the observed electron PSD (with speed less than ∼5000 km/s) shows a flat-topped shape in the direction along the local magnetic field.

4.2 6 February 1996 event (dusk tail-flank)

We study another event under prolonged but weakly northward IMF, where both electrons and cold proton component were less anisotropic than those in the previous event. On 6 February 1996, Geotail stayed in the plasma sheet near the dusk low-latitude boundary and observed the cold plasma sheet with two-component protons.

Figure 3 shows the solar wind observations by the Wind spacecraft between 00:00–15:00 UT. From the top, (a) the latitudinal angle of the IMF (θ_{IMF}), (b) the solar wind density (N_{SW}), and (c) the solar wind speed are plotted. After an extended southward IMF that continued for more than 12 h from the noon of the previous day, the IMF pointed weakly northward around 03:25 UT (Fig. 3a). The northward polarity of the IMF continued with the latitudinal angle of about 20–40 degrees, except for several short excursions toward the southward direction. The maximum value of θ_{IMF} in the 1-h averaged data is 41 degrees, which was observed between 10:00–11:00 UT. The solar-wind proton density and bulk

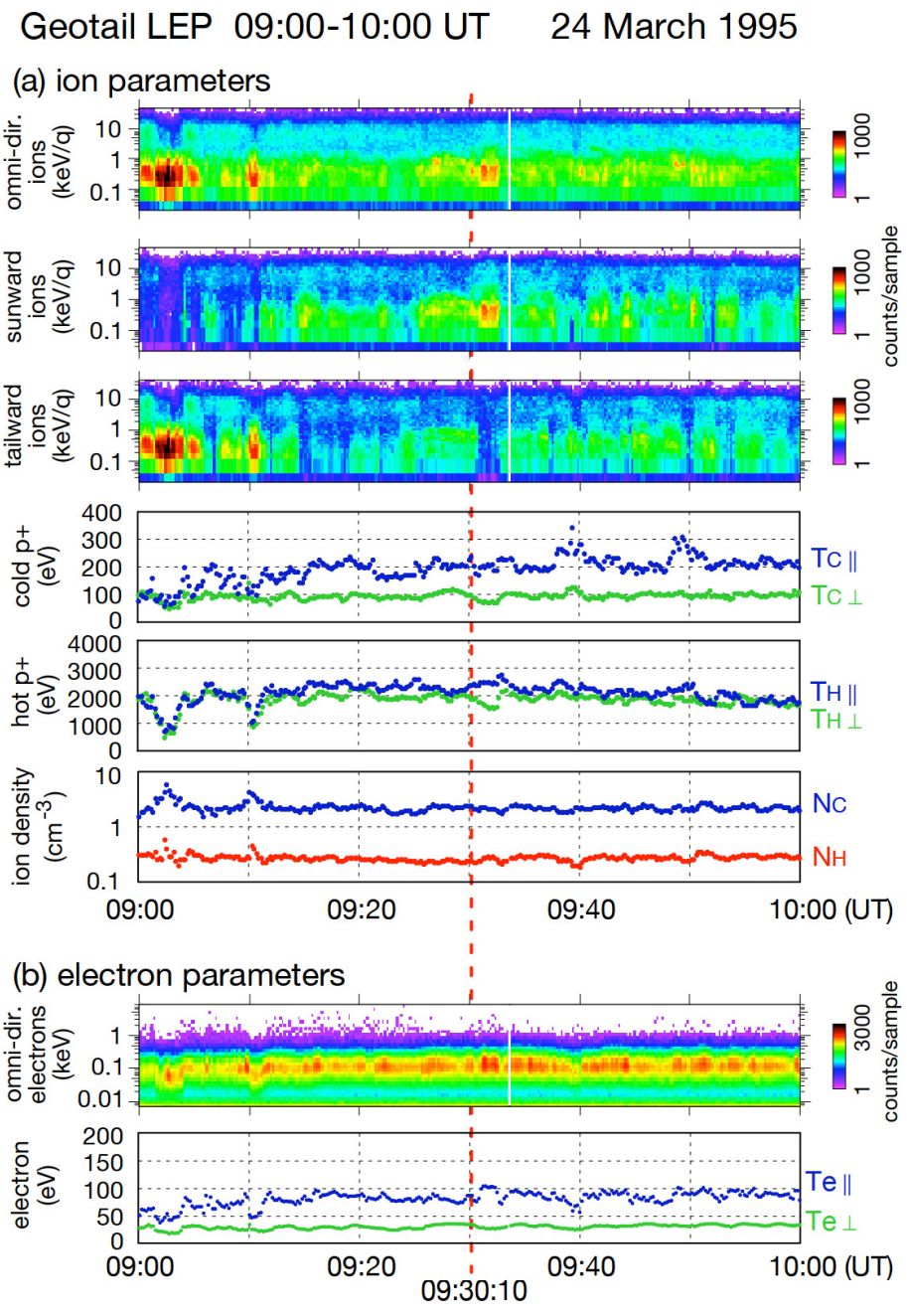

Fig. 1. Geotail observations between 09:00–10:00 UT on 24 March 1995. Panel **(a)** shows the ion observations. From the top, E-t spectrograms of omni-directional, sunward, and tailward ions, temperatures and densities of cold and hot proton components are presented. The perpendicular (parallel) temperature is shown by the green (blue) points, the density of the cold (hot) component is shown by the blue (red) points. Panel **(b)** shows the electron observations. E-t spectrogram of omni-directional electrons (7.4 eV–8.5 keV) and their temperatures are shown.

speed were 11.4 cm^{-3} and 360 km/s, respectively (Figs. 3b and c).

Figure 4 shows the Geotail observations between 11:00–15:00 UT in a similar format to Fig. 1 but the energy range of the electrons (LEP-EAe) is from 43 eV to 41.6 keV. At 12:00 UT Geotail was located at (−23.1, 19.4, −1.3) R_E in the GSM coordinates. In the following analysis, we focus on the interval 12:01–14:29 UT during which two components in the sunward and tailward E-t spectrograms are evident and the flows are stagnant ($|V_X|$<50 km/s).

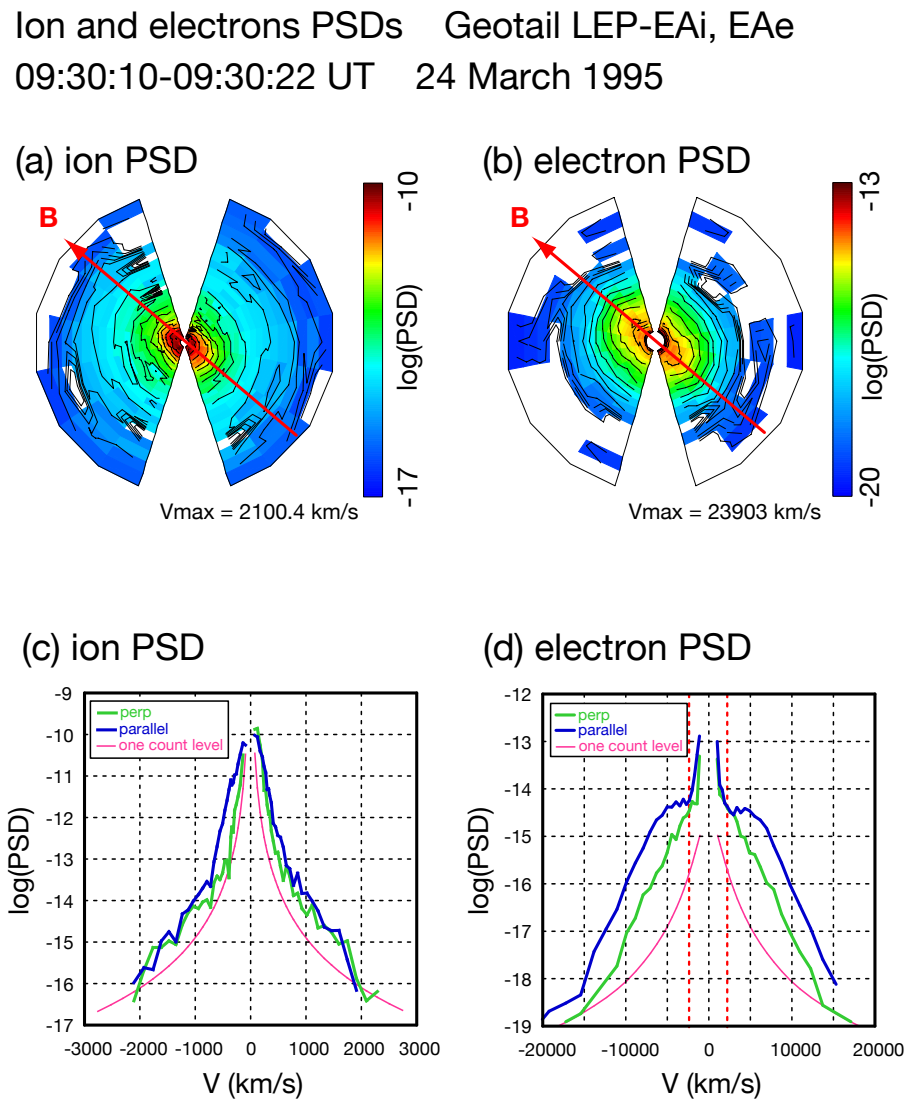

Fig. 2. Panel **(a)** shows a cut of ion PSD for the 12-s interval 09:30:10–09:30:22 UT on 24 March 1995, in the plane that includes the magnetic field. The field direction is shown by the red arrow. Panel **(b)** shows a cut of electron PSD for the same interval and in the same plane as shown in the left panel. Panels **(c)** and **(d)** show 1-D cuts of ion and electron PSDs in the direction perpendicular and parallel to the local magnetic field, which are shown by green and blue lines, respectively. A couple of vertical red broken lines in Panel (d) correspond to the lowest energy used for fitting calculations.

The cold proton component had a weak parallel anisotropy, $T_{C\perp}/T_{C\parallel}\sim0.84$, where averages of $T_{C\perp}$ and $T_{C\parallel}$ were 184 eV and 220 eV, respectively. The hot proton component was isotropic ($T_{H\perp}/T_{H\parallel}\sim1.0$), where both averages of $T_{H\perp}$ and $T_{H\parallel}$ were about 2.1–2.2 keV. Both $T_{H\perp}$ and $T_{H\parallel}$ gradually decreased from 2.6 keV to 1.5 keV, which is attributed to spatial and/or temporal variations of the plasma sheet. The average densities of the cold and hot proton components were about 0.94 cm^{-3} and 0.21 cm^{-3}, respectively. Before 12:00 UT the density of the cold component was less than 0.6 cm^{-3}, and around 12:04 UT it increased to be 0.9 cm^{-3}, while the density of the hot component was about 0.2 cm^{-3} and did not change around 12:00 UT. The density of the cold proton component dominated over that of the hot component, while thermal pressures of the hot component in the perpendicular and parallel directions (both ~70 pPa) were higher than those of the cold component (28 pPa and 33 pPa).

The electrons predominantly had a parallel anisotropy throughout the interval of the two-component proton observation. The average anisotropy of electrons was $T_{e\perp}/T_{e\parallel}\sim0.73$, where averages of $T_{e\perp}$ and $T_{e\parallel}$ were about 67 eV and 91 eV, respectively. In Fig. 4b we can find temporal and/or spatial variations of the electron temperatures; $T_{e\perp}$

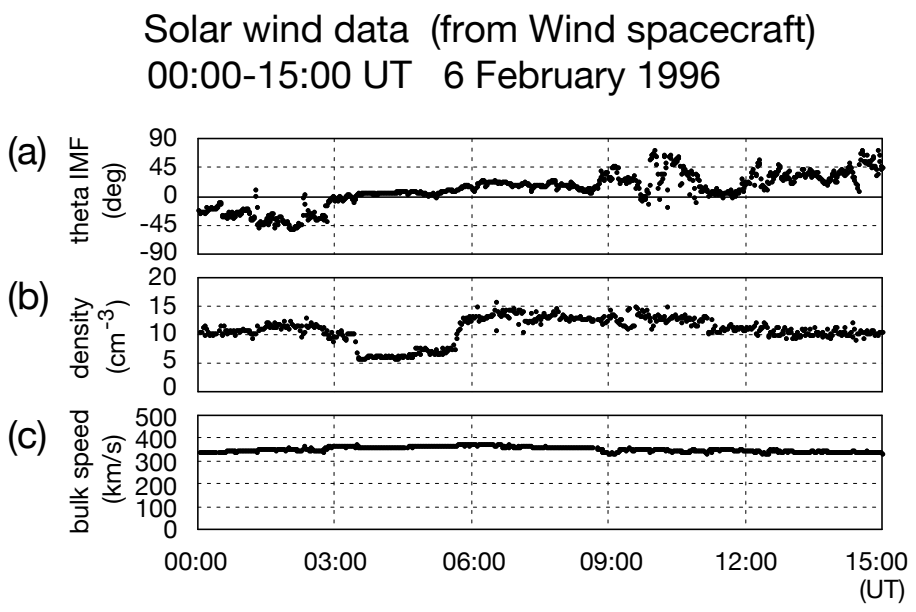

Fig. 3. Solar wind observations by the Wind spacecraft between 00:00–15:00 UT on 6 February 1996. From the top, **(a)** the latitudinal angle of the IMF ($\theta_{\rm IMF}$), **(b)** the solar wind density ($N_{\rm SW}$), and **(c)** the bulk speed of the solar wind flow ($V_{\rm SW}$) are presented. The convection time of the solar wind from the Wind to the Earth's magnetosphere ($\sim$1 h) is not included in the figure.

gradually increased and the parallel anisotropy gradually disappeared. The parallel anisotropy of electrons was strong ($T_{\rm e\perp}/T_{\rm e\parallel}\sim$0.5–0.7) between 12:01–12:56 UT. After 12:57 UT the anisotropy was weaker but the parallel temperature was still dominant ($T_{\rm e\perp}/T_{\rm e\parallel}\sim$0.8), except for several brief intervals when $T_{\rm e\perp}/T_{\rm e\parallel}$ was $\sim$1.1, and then the anisotropy gradually disappeared by 14:30 UT. The ratio of the cold-proton temperature to the electron temperature is about 2–3.

Figures 5a and b show PSDs of ions and electrons between 13:08:08–13:08:20 UT in a similar format to Figs. 2a and b, but the maximum speeds for ions and electrons are about 2300 km/s and 36 500 km/s, respectively. The magnetic field was ($-$3.1, $-$1.8, 3.6) nT in the GSM coordinates. The temperature anisotropies for the 12-s interval were $T_{\rm C\perp}/T_{\rm C\parallel}\sim$0.84, $T_{\rm H\perp}/T_{\rm H\parallel}\sim$1.1, and $T_{\rm e\perp}/T_{\rm e\parallel}\sim$0.58, where $T_{\rm C\perp}\sim$210 eV, $T_{\rm C\parallel}\sim$250 eV, $T_{\rm H\perp}\sim$2.3 keV, $T_{\rm H\parallel}\sim$2.1 keV, $T_{\rm e\perp}\sim$64 eV, and $T_{\rm e\parallel}\sim$110 eV. In Figs. 5a and b, elongations of PSD contours of cold protons and electrons are much weaker than those in the previous event (Figs. 2a and b). Figures 5c and d show 1-D cuts of PSDs of protons and electrons in the same format as Figs. 2c and d.

4.3 23 September 1995 event (dusk dayside)

We next proceed to a dusk-dayside event on 23 September 1995 to find that both cold and hot components of protons had a perpendicular anisotropy while electrons had a parallel anisotropy in contrast to the two previous cases in the tail-flank region.

The IMF pointed northward between 03:04–08:15 UT at the Wind location ($X\sim68\,R_E$), except for two short excursions to southward direction (see Nishino et al., 2007, for details). Near the end of the prolonged northward IMF period, Geotail crossed the dayside magnetopause from the magnetosheath into the magnetosphere. The solar wind speed was 386 km/s (0.77 keV) and its density was about 11.4 cm^{-3}. The convection time from the Wind location to the Earth's magnetosphere is roughly 20 min.

Figure 6 shows the Geotail observations between 07:30–08:10 UT in the same format as Fig. 4. Before 07:40 UT Geotail was in the dense magnetosheath-like region, and it came into the magnetosphere, crossing the dayside magnetopause around 07:41 UT when Geotail was located around (5.3, 9.1, $-$0.8) R_E in the GSM coordinates. Since the ion counts had two peaks in the energy space between 07:41–07:58 UT, we apply the two-Maxwellian mixture model to the ion PSD data for this interval. After 07:59 UT Geotail came into the hot plasma sheet, separating from the low-latitude boundary.

Nishino et al. (2007) found that both cold and hot components of protons in the plasma sheet had a perpendicular anisotropy in this event ($T_{\rm C\perp}/T_{\rm C\parallel}\sim$1.4 and $T_{\rm H\perp}/T_{\rm H\parallel}\sim$1.3). The perpendicular and parallel temperatures of the cold component ($T_{\rm C\perp}$ and $T_{\rm C\parallel}$) were 220 eV and 160 eV, and those of the hot component ($T_{\rm H\perp}$ and $T_{\rm H\parallel}$) were 4.5 keV and 3.4 keV, respectively. Since the average densities of the cold and hot components were about 2.0 cm^{-3} and 0.7 cm^{-3}, respectively, the cold component dominated over the hot one in terms of

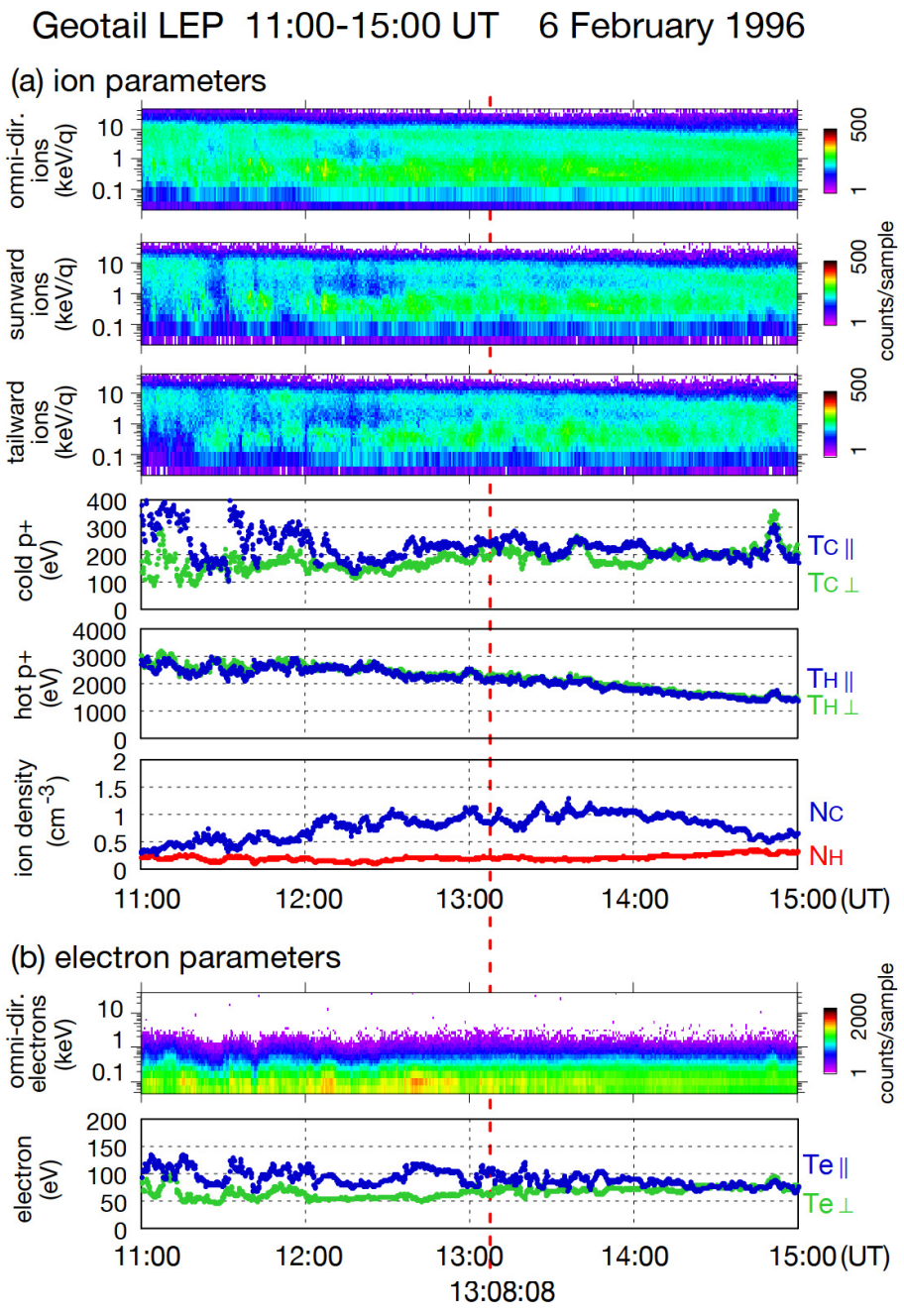

Fig. 4. Geotail observations between 11:00–15:00 UT on 6 February 1996 in a similar format to Fig. 1 but the energy range of the electron E-t spectrogram is from 43 eV to 41.6 keV.

the density. The thermal pressures of the hot component in the perpendicular and parallel directions (about 500 pPa and 380 pPa) dominated over those of the cold one (about 70 pPa and 50 pPa). In the plasma sheet adjacent to the boundary layer, both components were stagnant (<50 km/s).

We investigate the electron anisotropy in the plasma sheet for the interval of our interest (Fig. 6b). In contrast to the cold proton component with the perpendicular anisotropy, the electrons had a parallel anisotropy ($T_{e\perp}/T_{e\parallel}$~0.66). The perpendicular and parallel temperatures of the electrons ($T_{e\perp}$ and $T_{e\parallel}$) were 90 eV and 135 eV, respectively. In addition, we find that the cold electrons in the plasma sheet of our interest occasionally accompanied a high-energy (hot) component of electrons. In the E-t spectrogram of the electrons, hot electrons, whose energies are in the range of 1–10 keV, are occasionally seen (i.e. 07:41–07:44 UT, 07:46 UT, 07:47 UT,

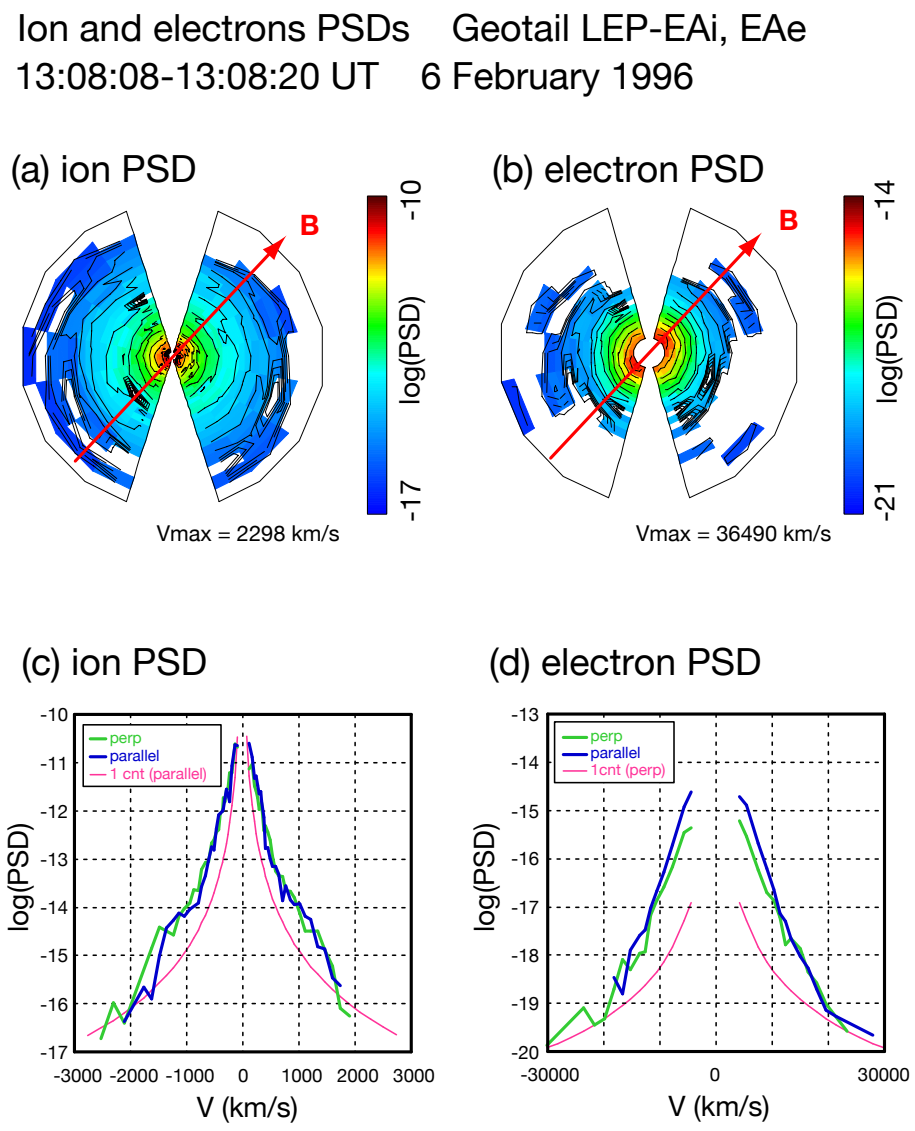

Fig. 5. Phase space densities of ions **(a)** and electrons **(b)** between 13:08:08–13:08:20 UT on 6 February 1996, in the plane that includes the local magnetic field. Panels **(c)** and **(d)** show 1-D cuts of ion and electron PSDs in the same format as Figs. 2c and d.

07:49 UT, 07:50–07:51 UT), although they were not observed for most of the interval. Since the energy range of the hot component resembles that of the thermal electrons in the plasma sheet observed after 07:59 UT, the hot component is thought to be of magnetospheric origin. The lack of the hot electron component is usually attributed to a leakage of hot electrons along the field line that was once opened to be connected to the IMF (Onsager et al., 2001).

Figure 7a (7b) shows a cut of ion (electron) PSD between 07:48:27–07:48:39 UT in a similar format to Fig. 2a (2b) but the maximum speed shown in the figure is about 2750 km/s (51 700 km/s). The magnetic field was (−2.7, 34.3, 30.6) nT in GSM. The temperature anisotropies for the 12-s interval were $T_{C\perp}/T_{C\parallel}\sim1.3$, $T_{H\perp}/T_{H\parallel}\sim1.2$, and $T_{e\perp}/T_{e\parallel}\sim0.62$, where $T_{C\perp}\sim170$ eV, $T_{C\parallel}\sim210$ eV, $T_{H\perp}\sim4.0$ keV, $T_{H\parallel}\sim3.4$ keV, $T_{e\perp}\sim73$ eV, and $T_{e\parallel}\sim120$ eV. Enhancement of the perpendicular anisotropy for the cold proton component is seen as the elongation of the PSD contours in the direction perpendicular to the magnetic field in Fig. 7a (yellow-red colored region). The parallel anisotropy of electrons is seen as the elongation of the PSD contours in the magnetic field direction in Fig. 7b. Figures 7c and d represent 1-D cuts of the phase space density of ions and electrons in the same format as Figs. 2c and d. Enhancement of the perpendicular component of the proton PSD is evident in Fig. 7c. In Fig. 7d, the parallel anisotropy of electrons is seen in the low energy range, while there is a high-energy component with a slight perpendicular anisotropy.

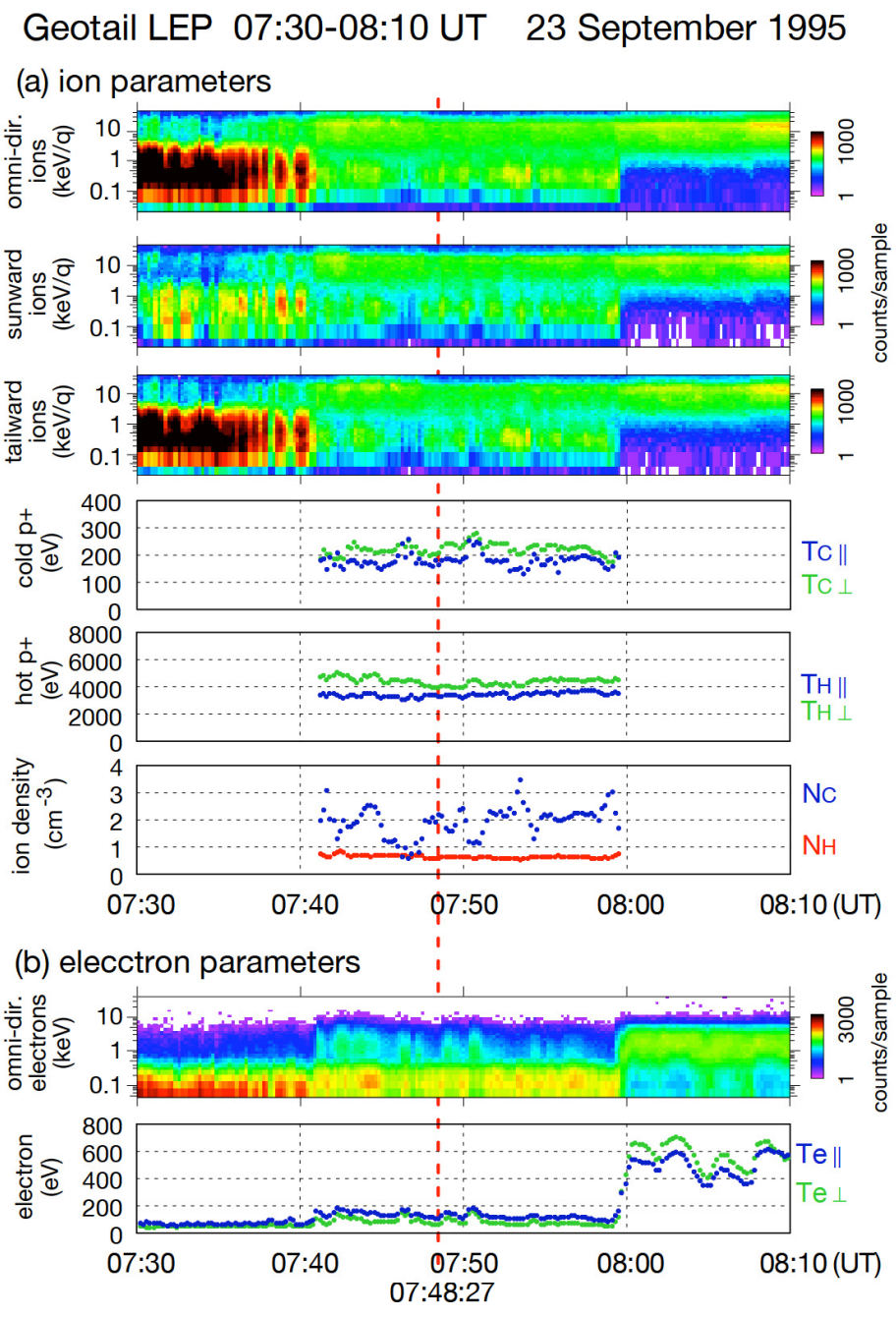

Fig. 6. Geotail observations between 07:30–08:10 UT on 23 September 1995 in the same format as Fig. 4.

5 Statistical study

According to the statistical study by Nishino et al. (2007), the sense of anisotropy of the cold proton component depends on the locations. On the other hand, the electrons have been known to possess a parallel anisotropy around the LLBL, with which the result of our case studies agrees. In addition, case studies performed above show that both anisotropies of electrons and the cold proton component change their strength in the tail flank. In order to further investigate the trend of the temperature anisotropies, we perform a statistical study as follows. In this paper we use the same data sets as Nishino et al. (2007); that is, the Geotail E-t spectrograms for the period 1995–2000 were scanned by eye and 15 intervals of the two-component protons, which consist of 11 in the tail and 4 on the dayside, were chosen. The relatively

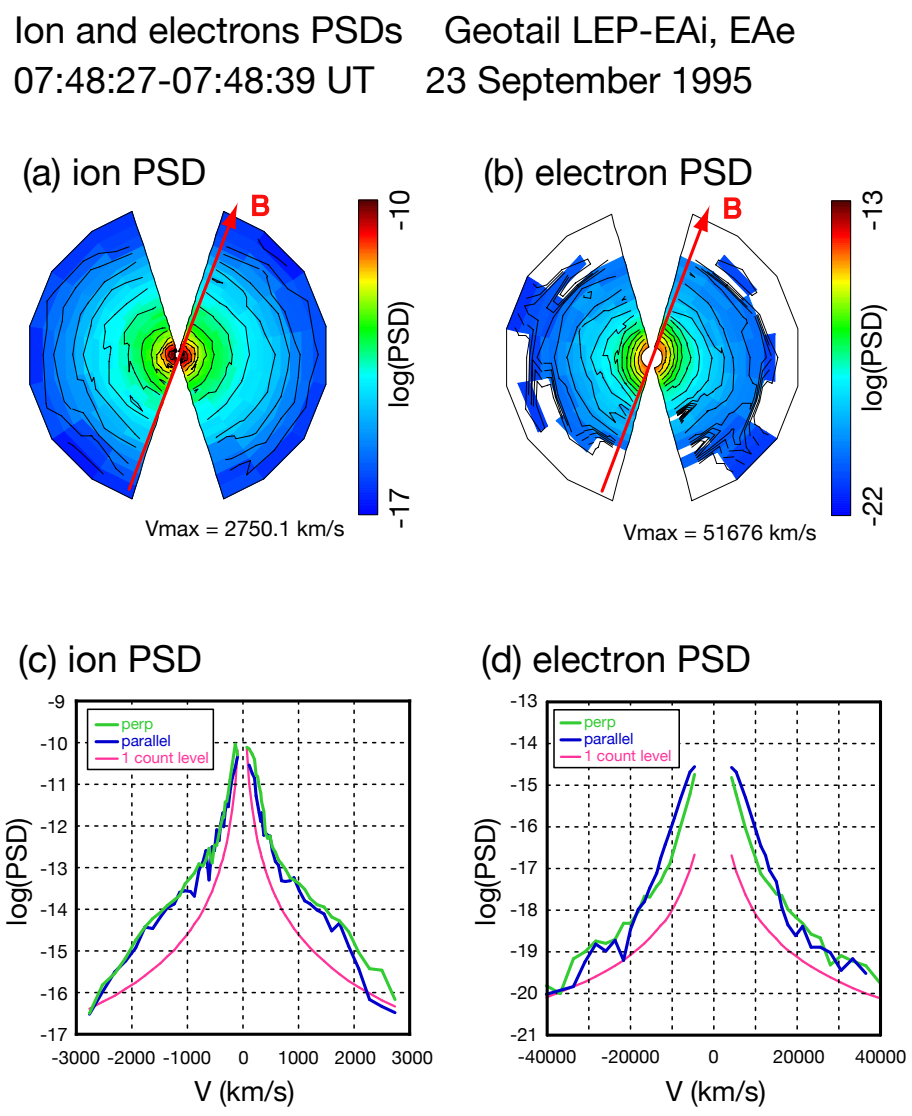

Fig. 7. Phase space densities of ions and electrons between 07:48:27–07:48:39 UT on 23 September 1995 in a similar format to Fig. 2.

small number of two-component events is due to the limited acquisition of 3-D data and to the seasonal change of the spacecraft orbit. The projection onto the XY (XZ) plane of the observed locations is shown in Fig. 8a (8b). The estimated parameters of each event are averaged over the intervals when the ion counts had two peaks and flows were stagnant ($|V_X|<50$ km/s). There was a continuous northward IMF period longer than 3 h just before each event, which is consistent with previous studies (e.g. Hasegawa et al., 2003; Nishino et al., 2005; Wing et al., 2005).

Figure 9a shows the anisotropy (the ratio of perpendicular to parallel temperature) of each component. The green squares, the blue triangles and the red plus symbols correspond to the anisotropies of electrons, and the cold and hot components of protons, respectively. Concerning the electrons, the ratio ($T_{e\perp}/T_{e\parallel}$) is in the range of 0.37–0.8, which means that both in the tail and on the dayside the electrons have a parallel anisotropy. The strongest parallel anisotropy is observed in the tail-flank plasma sheet between $X\sim-10$ and $-20\,R_E$. The spatial profile of temperature anisotropies of protons differs from that of electrons. As was shown by Nishino et al. (2007), the sense of the temperature anisotropy of the cold proton component ($T_{C\perp}/T_{C\parallel}$) depends on the X coordinate of the observed location (Fig. 9a). The strong parallel anisotropy of the cold component is occasionally observed around $X\sim-10$ to $\sim-20\,R_E$, being accompanied by the strong parallel anisotropy of electrons. Nishino et al. (2007) pointed out that the hot proton component is less anisotropic than the cold component in the tail flank, and has a perpendicular anisotropy in the dayside region. The

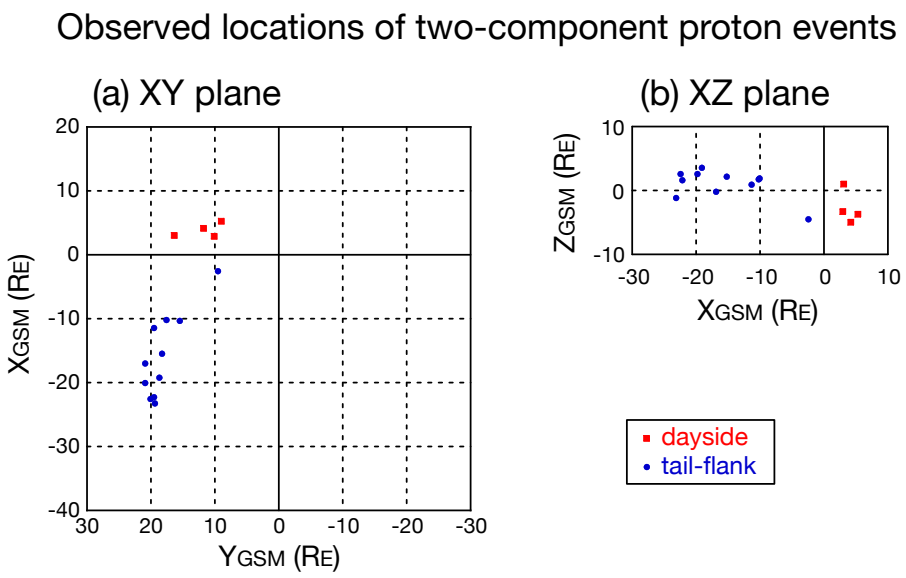

Fig. 8. Observed locations of the plasma sheet with the two-component protons near the dusk low-latitude boundary. Projections onto **(a)** the GSM *XY* plane and **(b)** the GSM *XZ* plane are shown. Dayside (tail) events are plotted as red squares (blue circles).

perpendicular anisotropy of the hot proton component may be due to the result of adiabatic transport from the tail region and losses into the ionosphere, as is usual in the plasma sheet (Mauk and McPherron, 1980).

Figure 9b shows the perpendicular and parallel temperatures of electrons normalized by the kinetic energy of solar wind protons (E_{SW}). The green squares (blue circles) correspond to the normalized perpendicular (parallel) temperature. The larger variation of the parallel temperature than the perpendicular temperature could be attributed to some parallel heating process.

Let us compare the temperatures of electrons with those of the cold proton component. The perpendicular and parallel temperatures of the cold proton component normalized by E_{SW} are shown in Fig. 9c. Most of the temperatures of the cold component are in the range of 20–40 percent of the kinetic energy of the solar wind protons. Comparing Figs. 9b and 9c, we find that temperatures of the cold proton component are roughly twice as high as those of electrons. The typical temperature ratio of protons to electrons is about 7 in the near-Earth plasma sheet (Baumjohann, 1993), and therefore, selective heating works on protons in the plasma sheet. The observed temperature ratio in the cold plasma sheet means that the cold proton component does not significantly receive selective heating during the cold plasma sheet formation.

Comparing the normalized temperatures of the hot proton component (Fig. 9d) to the normalized electron temperatures (Fig. 9b), we note that the temperature ratio of the hot proton component to the electrons can be as large as 20, which may be attributed to escape of the high-energy electrons along the open (or once-opened) field line.

Figure 10a shows the relation between the latitudinal angle of the IMF (θ_{IMF}) and anisotropies of the electrons and the cold and hot proton components for the 11 tail-flank events. Green squares, blue triangles, and red plus symbols correspond to the anisotropies of the electrons, the cold proton component, and the hot proton component, respectively. For the data of the latitudinal angle of the IMF, we use the maximum value of the 1-h averaged data within 6 h before the detection of the two-component protons. There is a trend that strongly northward IMF leads to strong parallel anisotropies of both electrons and the cold proton component in the tail flank region. The parallel anisotropy of electrons is stronger than that of the cold proton component, which is stronger than that of the hot proton component; i.e. there is a relation $T_{e\perp}/T_{e\parallel} < T_{C\perp}/T_{C\parallel} < T_{H\perp}/T_{H\parallel}$ in the tail-flank plasma sheet with two-component protons.

On the other hand, no dependence of anisotropies on the strength of the northward IMF can be found in the dayside events. Figure 10b shows the relation between θ_{IMF} and anisotropies for the 4 dayside events. The electrons have a strong parallel anisotropy, being independent of the latitudinal angle of the IMF, while both proton components have perpendicular anisotropies.

Figures 10c and d show relations between the electron anisotropy and the proton anisotropies in the tail flank and on the dayside, respectively. The blue triangles correspond to the anisotropy of the cold proton component, and red plus symbols designate the hot proton component. In the tail flank, the anisotropy of electrons is in a good correlation with that of the cold proton component, with a correlation coefficient of 0.87, while it is not correlated with that of the hot

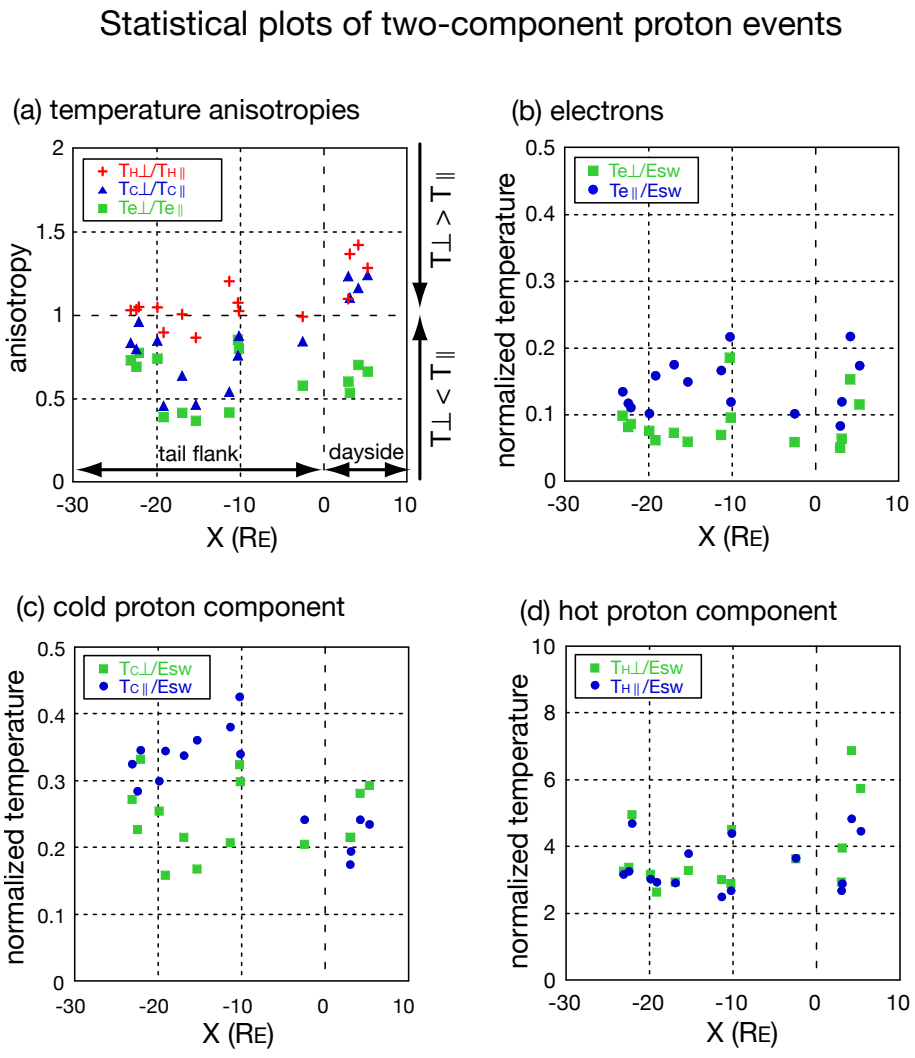

Fig. 9. Statistical plots for the 4 dayside and 11 tail events. Panel **(a)** shows anisotropies (i.e. ratios of perpendicular to parallel temperature) of the cold protons, the hot protons, and the electrons. The blue (red) points correspond to the ratio of the cold (hot) component temperatures, and the green squares represent the electron temperatures. Panels **(b–d)** show the relation between the X coordinate of the observed locations and the temperatures normalized by the kinetic energy by the solar wind protons (437.7 km/s=1 keV). Panel (b) shows the normalized temperatures of electrons in the perpendicular and parallel direction to the magnetic field, with green squares (blue circles) corresponding to the perpendicular (parallel) temperature. Panels (c) and (d) present the normalized temperatures of the cold and hot proton components, respectively.

proton component. As for the cases on the dayside, we cannot judge whether there is a correlation between the electron anisotropy and the proton anisotropies because of the narrow range of the observed anisotropies.

6 Discussion

In order to discuss what findings in the present study mean, we first summarize the results and suggestions of the study by Nishino et al. (2007). Focusing on the two-component protons in the dusk plasma sheet, Nishino et al. (2007) pointed out that the sense of anisotropy of the cold proton component depends on the observed locations; the cold proton component possesses a parallel anisotropy in the tail ($T_{C\perp}/T_{C\parallel}<1$) and a perpendicular anisotropy on the dayside ($T_{C\perp}/T_{C\parallel}>1$). What they found suggests that the cold proton component on the dayside and in the tail flank region came into the magnetosphere through separate locations, and implies that a different entry mechanism works on the dayside and in the tail flank. They mentioned that the kinetic Alfvén waves (KAWs) are not inconsistent with the observed perpendicular anisotropy of the cold proton component on the dayside,

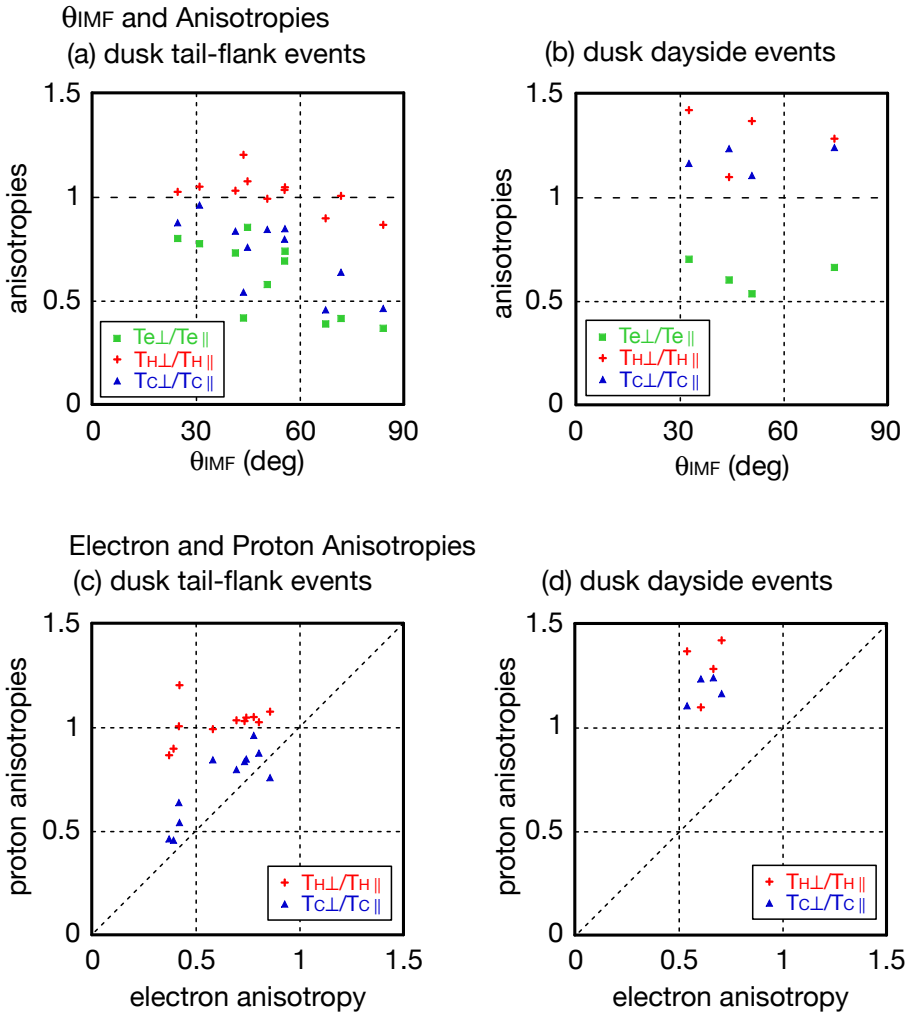

Fig. 10. Statistical plots of observed temperature anisotropies. The top two panels show the dependence of the anisotropies on the IMF latitudinal angle (θ_{IMF}) for **(a)** tail-flank events and **(b)** dayside events. The bottom two panels present the relation between electron anisotropy and proton anisotropies for **(c)** the tail-flank and **(d)** the dayside events. Green squares, blue triangles, and red plus symbols correspond to the anisotropies of the electrons, the cold proton component, and the hot proton component, respectively.

since the KAWs can heat ions in the direction perpendicular to the local magnetic field (Johnson and Cheng, 1997). Concerning the cold proton component in the tail flank (Fig. 9c), they proposed that the enhancement of the parallel temperature in the tail flank might be partly attributed to adiabatic heating due to earthward convection in the plasma sheet. The adiabatic heating is a result of the interplay between betatron and Fermi accelerations, and the parallel temperature is enhanced as the result of earthward convection in the region with the tail-like magnetic field configuration (Yamamoto and Tamao, 1978).

Let us discuss a plausible mechanism on the dayside. In the present study, we have confirmed that the cold electrons possess a parallel anisotropy ($T_{e\perp}/T_{e\parallel}<1$) on the dayside where the the cold proton component has a perpendicular anisotropy. Since the KAWs can explain both the electron heating in the parallel direction and ion heating in the perpendicular direction (Johnson and Cheng, 1997; Johnson et al., 2001), the KAWs around the dayside magnetopause might explain the observed anisotropies, although we have not obtained direct evidence of the KAW's excitation in our data.

Another candidate for solar wind entry and heating under (strongly) northward IMF is double high-latitude reconnection at the dayside magnetopause (Song and Russell, 1992; Li et al., 2005; Øieroset et al., 2005). Previous observational studies (Onsager et al., 2001; Lavraud et al., 2005, 2006) showed that electrons on the newly-closed field lines around the dayside magnetopause possess a parallel anisotropy, consistent with our observations on the dayside.

In the tail flank region a good correlation between the parallel anisotropy of electrons and that of the cold proton component supports the idea of the adiabatic heating, for both electrons and protons undergo the same sense of heating as long as they move together on the same field line. However, the observed parallel anisotropy of electrons is stronger than that of the cold proton component in the tail flank, which means that adiabatic change by itself cannot totally explain the observed anisotropies and that some other mechanism of parallel heating acts on the electrons. The observed dependence of parallel anisotropies in the tail flank on the latitudinal angle of the IMF ($\theta_{\rm IMF}$) also implies an additional mechanism other than adiabatic heating.

We consider roles of Kelvin-Helmholtz (KH) instability in plasma heating around the magnetopause. In the velocity shear layer around the magnetopause, the Kelvin-Helmholtz (KH) instability is expected to develop under strongly northward IMF (Fairfield et al., 2000). Simulations (Otto and Fairfield, 2000; Nykyri and Otto, 2001; Matsumoto and Hoshino, 2006; Nakamura et al., 2006), as well as observational studies (Hasegawa et al., 2004, 2006), have suggested the occurrence of KH instability and growth of vortical structures there. We note that the two events with the strong parallel anisotropy of the cold proton component in the tail flank ($T_{\rm C\perp}/T_{\rm C\parallel}<0.5$ on 24 March 1995 and 13 April 1998) are those where Hasegawa et al. (2006) showed the existence of the rolled-up KH vortical structures, and that other 9 tail-flank cases with the weaker parallel anisotropy were not identified as the rolled-up KH vortices by them. As for the event on 24 March 1995, Fairfield et al. (2000) and Otto and Fairfield (2000) performed a comparison between the Geotail data and MHD simulations, and concluded that the low-latitude boundary on the duskside was unstable to the KH instability. We therefore propose that the strong parallel anisotropies may be related to the KH vortical structures developed under strongly northward IMF. Furthermore, recent simulation studies (e.g. Otto and Fairfield, 2000; Nykyri and Otto, 2001; Nakamura et al., 2006) showed that magnetic reconnection occurs in the KH vortical structures and plays an important role in plasma transport across the magnetopause. If magnetic reconnection occurs in the KH vortices around the magnetopause, it might explain the enhancement of parallel temperatures of the electrons and the cold proton component ($T_{\rm e\parallel}$ and $T_{\rm C\parallel}$) around $X\sim-10$ to $\sim-20\,R_E$. Recently, Nykyri et al. (2006) reported that a double-population distribution function of the cold proton component was observed in the low-latitude boundary on the dawnside, and they discussed that the double population is likely to be a signature of magnetic reconnection due to the KH instability. Such a distribution function might be related to the parallel anisotropy of the cold proton component in the present study. In addition to magnetic reconnection, a large fluctuation of the magnetic field in the KH vortices might generate KAWs that result in parallel heating of electrons (Sibeck et al., 1999).

Other waves, such as the electric solitary wave (ESW) and the lower-hybrid drift wave (LHDW), are also candidates for serving as a plasma heating mechanism around the magnetopause. The ESW has been known to lead to electron heating (Omura et al., 1996; Goldman et al., 1999) and was observed at the magnetopause under northward IMF (Cattell et al., 2002). The LHDW has also been proposed as a plasma transport mechanism across the magnetopause (Treumann et al., 1991; Shukla and Mamun, 2002). Since the LHDW might play an important role in the formation of the flat-topped electrons in the magnetotail (Shinohara and Hoshino, 1999; Shinohara et al., 2001), the LHDW around the magnetopause, if any, might produce the flat-topped electrons observed on 24 March 1995. Further studies of wave-particle interactions, as well as distribution functions, in detail, may help us understand what is going on around the magnetopause under northward IMF.

7 Conclusions

We have found that both electrons and protons have temperature anisotropy in the cold plasma sheet. The electrons have a parallel anisotropy both on the dayside and in the tail flank, while the sense of the anisotropy of the cold proton component depend on the locations. Although the observed parallel anisotropies of the electrons and the cold proton component in the tail flank may be partly explained by adiabatic heating by earthward convection in the plasma sheet, some other mechanism that selectively heats electrons in the parallel direction may work. Strong parallel anisotropies observed under strongly northward IMF may be attributed to the development of Kelvin-Helmholtz vortices in the tail flank and the resultant magnetic reconnection in the vortical structures. Wave-particle interactions are also candidates for plasma transport and heating around the magnetopause.

Acknowledgements. We thank T. Nagai for providing the magnetic field data from the MGF instrument on board Geotail spacecraft. We also thank the principal investigators of ACE MAG and SWEPAM experiments and Wind MFI and SWE instruments for providing the solar wind data via CDAWeb. M. N. Nishino thanks H. Hasegawa, Y. Seki, and I. Shinohara for fruitful discussion.

Topical Editor I. A. Daglis thanks two anonymous referees for their help in evaluating this paper.

References

Baumjohann, W.: The near-Earth plasma sheet: An AMPTE/IRM perspective, Space Sci. Rev., 64, 141–163, doi:10.1007/BF00819660, 1993.

Borovsky, J. E., Thomsen, M. F., and Elphic, R. C.: The driving of the plasma sheet by the solar wind, J. Geophys. Res., 103(A8), 17 617–17 639, 1998.

Cattell, C., Crumley, J., Dombeck, J., and Wygant, J.: Polar observations of solitary waves at the Earth's magnetopause, Geophys. Res. Lett., 29, 1065, doi:10.1029/2001GL014046, 2002.

Cowley, S. W. H. and Ashour-Abdalla, M.: Adiabatic plasma convection in a dipole field: Variation of plasma bulk parameters with L, Planet. Space Sci., 23(11), 1527–1549, doi:10.1016/0032-0633(75)90006-9, 1975.

Eastman, T. E., Hones Jr., E. W., Bame, S. J., and Asbridge, J. R.: The magnetospheric boundary layer: Site of plasma, momentum, and energy transfer from the magnetosheath into the magnetosphere, Geophys. Res. Lett., 3, 685–688, 1976.

Fairfield, D. H., Otto, A., Mukai, T., Kokubun, S., Lepping, R. P., Steinberg, J. T., Lazarus, A. J., and Yamamoto, T.: Geotail observations of the Kelvin-Helmholtz instability at the equatorial magnetotail boundary for parallel northward fields, J. Geophys. Res., 105(A9), 21 159–21 174, doi:10.1029/1999JA000316, 2000.

Fujimoto, M., Terasawa, T., Mukai, T., Saito, Y., Yamamoto, T., and Kokubun, S.: Plasma entry from the flanks of the near-Earth magnetotail: Geotail observations, J. Geophys. Res., 103, 4391–4408, 1998.

Gary S. P., Lavraud, B., Thomsen, M. F., Lefebvre, B., and Schwartz, S. J.: Electron anisotropy constraint in the magnetosheath: Cluster observations, Geophys. Res. Lett., 32, L13109, doi:10.1029/2005GL023234, 2005.

Goldman, M. V., Oppenheim, M. M., and Newman, D. L.: Nonlinear two-stream instabilities as an explanation for auroral bipolar wave structures, Geophys. Res. Lett., 26(13), 1821–1824, doi:10.1029/1999GL900435, 1999.

Hada, T., Nishida, A., Terasawa, T., and Hones Jr., E. W.: Bidirectional electron pitch angle anisotropy in the plasma sheet, J. Geophys. Res., 86, 11 211–11 224, 1981.

Hasegawa, H., Fujimoto, M., Maezawa, K., Saito, Y., and Mukai, T.: Geotail observations of the dayside outer boundary region: Interplanetary magnetic field control and dawn-dusk asymmetry, J. Geophys. Res., 108(A4), 1163, doi:10.1029/2002JA009667, 2003.

Hasegawa, H., Fujimoto, M., Phan, T.-D., Rème, H., Dunlop, M. W., Hashimoto, C., and TanDokoro, R.: Transport of solar wind into Earth's magnetosphere through rolled-up Kelvin-Helmholtz vortices, Nature, 430, 755–758, 2004.

Hasegawa, H., Fujimoto, M., Takagi, K., Saito, Y., Mukai, T., and Rème, H.: Single-spacecraft detection of rolled-up Kelvin-Helmholtz vortices at the flank magnetopause, J. Geophys. Res., 111, A09203, doi:10.1029/2006JA011728, 2006.

Ishisaka, K., Okada, T., Tsuruda, K., Hayakawa, H., Mukai, T., and Matsumoto, H.: Relationship between the Geotail spacecraft potential and the magnetospheric electron number density including the distant tail regions, J. Geophys. Res., 106(A4), 6309–6320, doi:10.1029/2000JA000077, 2001.

Johnson, J. R. and Cheng, C. Z.: Kinetic Alfvén waves and plasma transport at the magnetopause, Geophys. Res. Lett., 24(11), 1423–1426, doi:10.1029/97GL01333, 1997.

Johnson, J. R., Cheng, C. Z., and Song, P.: Signatures of mode conversion and kinetic Alfvén waves at the magnetopause, Geophys. Res. Lett., 28, 227–230, doi:10.1029/2000GL012048, 2001.

Kokubun, S., Yamamoto, T., Acuña, M. H., Hayashi, K., Shiokawa, K., and Kawano, H.: The GEOTAIL magnetic field experiment, J. Geomag. Geoelectr., 46, 7–21, 1994.

Lavraud, B., Thomsen, M. F., Taylor, M. G. G. T., Wang, Y. L., Phan, T. D., Schwartz, S. J., Elphic, R. C., Fazakerley, A., Rème, H., and Balogh, A.: Characteristics of the magnetosheath electron boundary layer under northward interplanetary magnetic field: Implications for high-latitude reconnection, J. Geophys. Res., 110, A06209, doi:10.1029/2004JA010808, 2005.

Lavraud, B., Thomsen, M. F., Lefebvre, B., Schwartz, S. J., Seki, K., Phan, T. D., Wang, Y. L., Fazakerley, A., Rème, H., and Balogh, A.: Evidence for newly closed magnetosheath field lines at the dayside magnetopause under northward IMF, J. Geophys. Res., 111, A05211, doi:10.1029/2005JA011266, 2006.

Lepping, R. P., Acuña, M., Burlaga, L., Farrell, W., Slavin, J., Schatten, K., Mariani, F., Ness, N., Neubauer, F., Whang, Y. C., Byrnes, J., Kennon, R., Panetta, P., Scheifele, J., and Worley, E.: The WIND Magnetic Field Investigation, Space Sci. Rev., 71, 207–229, 1995.

Li, W., Raeder, J., Dorelli, J., Øieroset, M., and Phan, T. D.: Plasma sheet formation during long period of northward IMF, Geophys. Res. Lett., 32, L12S08, doi:10.1029/2004GL021524, 2005.

Matsumoto, Y. and Hoshino, M.: Turbulent mixing and transport of collisionless plasmas across a stratified velocity shear layer, J. Geophys. Res., 111, A05213, doi:10.1029/2004JA010988, 2006.

Mauk, B. H. and McPherron, R. L.: An experimental test of the electromagnetic ion cyclotron instability within the earth's magnetosphere, Phys. Fluids, 23, 2111–2127, 1980.

McComas, D. J., Bame, S. J., Barker, P., Feldman, W. C., Phillips, J. L., Riley, P., and Griffee, J. W.: Solar Wind Electron Proton Alpha Monitor (SWEPAM) for the Advanced Composition Explorer, Space Sci. Rev., 86, 563–612, 1998.

Mukai, T., Machida, S., Saito, Y., Hirahara, H., Terasawa, T., Kaya, N., Obara, T., Ejiri, M., and Nishida, A.: The Low Energy Particle (LEP) experiment onboard the GEOTAIL satellite, J. Geomag. Geoelectr., 46, 669–692, 1994.

Nakamura, T. K. M., Fujimoto, M., and Otto, A.: Magnetic reconnection induced by weak Kelvin-Helmholtz instability and the formation of the low-latitude boundary layer, Geophys. Res. Lett., 33, L14106, doi:10.1029/2006GL026318, 2006.

Nishino, M. N., Terasawa, T., and Hoshino, M.: Increase of the tail plasma content during the northward interplanetary magnetic field intervals: Case studies, J. Geophys. Res., 107(A9), 1261, doi:10.1029/2002JA009268, 2002.

Nishino, M. N., Terasawa, T., and Hoshino, M.: Geotail observations of the cold plasma sheet on the duskside magnetotail, Frontiers of Magnetospheric Plasma Physics, Celebrating 10 Years of Geotail Oparation, COSPAR Colloquia Series Volume 16, 28–33, 2005.

Nishino, M. N., Fujimoto, M., Terasawa, T., Ueno, G., Maezawa, K., Mukai, T., and Saito, Y.: Geotail observations of temperature anisotropy of the two-component protons in the dusk plasma sheet, Ann. Geophys., 25, 769–777, 2007, http://www.ann-geophys.net/25/769/2007/.

Nykyri, K. and Otto, A.: Plasma transport at the magnetospheric boundary due to reconnection in Kelvin-Helmholtz vortices, Geophys. Res. Lett., 28(18), 3565–3568, doi:10.1029/2001GL013239, 2001.

Nykyri, K., Otto, A., Lavraud, B., Mouikis, C., Kistler, L. M., Balogh, A., and Rème, H.: Cluster observations of reconnection due to the Kelvin-Helmholtz instability at the dawnside magnetospheric flank, Ann. Geophys., 24, 2619–2643, 2006, http://www.ann-geophys.net/24/2619/2006/.

Ogilvie, K. W., Chornay, D. J., Fritzenreiter, R. J., Hunsaker, F., Keller, J., Lobell, J., Miller, G., Scudder, J. D., Sittler, E. C., Torbert, R. B., Bodet, D., Needell, G., Lazarus, A. J., Steinberg, J.

T., Tappan, J. H., Mavretic, A., and Gergin, E.: SWE, A comprehensive plasma instrument for the Wind spacecraft, Space Sci. Rev., 71, 55–77, doi:10.1007/BF00751326, 1995.

Øieroset, M., Raeder, J., Phan, T. D., Wing, S., McFadden, J. P., Li, W., Fujimoto, M., Rème, H., and Balogh, A.: Global cooling and densification of the plasma sheet during an extended period of purely northward IMF on October 22–24, 2003, Geophys. Res. Lett., L12S07, doi:10.1029/2004GL021523, 2005.

Omura, Y., Matsumoto, H., Miyake, T., and Kojima, H.: Electron beam instabilities as generation mechanism of electrostatic solitary waves in the magnetotail, J. Geophys. Res., 101(A2), 2685–2697, 10.1029/95JA03145, 1996.

Onsager, T. G., Scudder, J. D., Lockwood, M., and Russell, C. T.: Reconnection at the high-latitude magnetopause during northward interplanetary magnetic field conditions, J. Geophys. Res., 106(A11), 25 467–25 488, doi:10.1029/2000JA000444, 2001.

Otto, A. and Fairfield, D. H.: Kelvin-Helmholtz instability at the magnetotail boundary: MHD simulation and comparison with Geotail observations, J. Geophys. Res., 105(A9), 21 175–21 190, doi:10.1029/1999JA000312, 2000.

Phan, T. D., Larson, D. E., Lin, R. P., McFadden, J. P., Anderson, K. A., Carlson, C. W., Ergun, R. E., Ashford, S. M., McCarthy, M. P., Parks, G. K., Rème, H., Bosqued, J. M., D'Uston, C. D., Wenzel, K.-P., Sanderson, T. R., and Szabo, A.: The subsolar magnetosheath and magnetopause for high solar wind ram pressure: WIND observations, Geophys. Res. Lett., 23(10), 1279–1282, 1996.

Phan, T. D., Larson, D., McFadden, J., Lin, R. P., Carlson, C., Moyer, M., Paularena, K. I., McCarthy, M., Parks, G. K., Rème, H., Sanderson, T. R., and Lepping, R. P.: Low-latitude dusk flank magnetosheath, magnetopause, and boundary layer for low magnetic shear: Wind observations, J. Geophys. Res., 102(A9), 19 883–19 896, doi:10.1029/97JA01596, 1997.

Sckopke, N., Paschmann, G., Haerendel, G., Sonnerup, B. U. Ö., Bame, S. J., Forbes, T. G., Hones Jr., E. W., and Russell, C. T.: Structure of the low-latitude boundary layer, J. Geophys. Res., 86, 2099–2110, 1981.

Shinohara, I. and Hoshino, M.: Electron heating process of the lower hybrid drift instability, Adv. Space Res., 24, 43–46, 1999.

Shinohara, I., Suzuki, H., Fujimoto, M., and Hoshino, M.: Rapid large scale magnetic field dissipation in a collisionless current sheet via coupling between Kelvin-Helmholtz and lower hybrid drift instabilities, Phys. Rev. Lett., 87, 95001, doi:10.1103/RphysRevLett.87.095001, 2001.

Shiokawa, K., Baumjohann, W., and Paschmann, G.: Bi-directional electrons in the near-Earth plasma sheet, Ann. Geophys., 21, 1497–1507, 2003, http://www.ann-geophys.net/21/1497/2003/.

Shukla, P. K. and Mamun, A. A.: Lower hybrid drift wave turbulence and associated electron transport coefficients and coherent structures at the magnetopause boundary layer, J. Geophys. Res., 107(A11), 1401, doi:10.1029/2002JA009374, 2002.

Sibeck, D. G., Paschmann, G., Treumann, R. A., Fuselier, S. A., Lennartsson, W., Lockwood, M., Lundin, R., Ogilvie, K. W., Onsager, T. G., Phan, T.-D., Roth, M., Scholer, M., Sckopke, N., Stasiewicz, K. and Yamauchi, M.: Chapter 5– Plasma transfer processes at the magnetopause, in Magnetospheric plasma sources and losses, Space Sci. Rev., 88(1–2), 207–283, doi:10.1023/A:1005255801425, 1999.

Smith, C. W., Acuña, M. H., Burlaga, L. F., L'Heureux, J., Ness, N. F., and Scheifele, J.: The ACE magnetic field experiment, Space Sci. Rev., 86, 613–632, 1998.

Song, P. and Russell, C. T.: Model of the formation of the low-latitude boundary layer for strongly northward interplanetary magnetic field, J. Geophys. Res., 97(A2), 1411–1420, 1992.

Sugiyama, T., Fujimoto, M., Nagai, T., Mukai, T., Saito, Y., Terasawa, T., Yamamoto, T., and Kokubun, S.: Highly collimated electron beams observed during quiet times, Geophys. Res. Lett., 24(13), 1651–1654, 1997.

Terasawa, T., Fujimoto, M., Mukai, T., Shinohara, I., Saito, Y., Yamamoto, T., Machida, S., Kokubun, S., Lazarus, A. J., Steinberg, J. T., and Lepping, R. P.: Solar wind control of density and temperature in the near-Earth plasma sheet: Wind/Geotail collaboration, Geophys. Res. Lett., 24, 935–938, 1997.

Traver, D. P., Mitchell, D. G., Williams, D. J., Frank, L. A., and Huang, C. Y.: Two encounters with the flank low-latitude boundary layer: Further evidence for closed field topology and investigation of the internal structure, J. Geophys. Res., 96(A12), 21 025–21 035, 1991.

Treumann, R. A., Labelle, J., and Pottelette, R.: Plasma diffusion at the magnetopause – The case of lower hybrid drift waves, J. Geophys. Res., 96(A9), 16 009–16 013, doi:10.1029/91JA01671, 1991.

Treumann, R. A. and Baumjohann, W.: Advanced Space Plasma Physics, Imperial College Press, London, 1997.

Ueno, G., Nakamura, N., Higuchi, T., Tsuchiya, T., Machida, S., Araki, T., Saito, Y., and Mukai, T.: Application of multivariate Maxwellian mixture model to plasma velocity distribution function, J. Geophys. Res., 106(A11), 25 655–25 672, 2001a.

Ueno, G., Nakamura, N., and Higuchi, T.: Separation of photoelectrons via multivariate Maxwellian mixture model, Lecture Notes in Computer Science, vol. 2226, edited by: Jantke, K. P. and Shinohara, A., pp. 470–475, Springer-Verlag Berlin Heidelberg, 2001b.

Wing, S., Johnson, J. R., Newell, P. T., and Meng, C.-I.: Dawn-dusk asymmetries, ion spectra, and sources in the northward interplanetary magnetic field plasma sheet, J. Geophys. Res., 110, A08205, doi:10.1029/2005JA011086, 2005.

Yamamoto, T. and Tamao, T.: Adiabatic plasma convection in the tail plasma sheet, Planet. Space Sci., 26, 1185–1191, doi:10.1016/0032-0633(78)90058-2, 1978.

Zwolakowska, D., Koperski, P., and Popielawska, B.: Plasma populations in the tail during northward IMF, Proceedings of the international conference on substorms (ICS-1), ESA SP-335, 57–62, 1992.

Zwolakowska, D. and Popielawska, B.: Tail plasma domains and the auroral oval: results of mapping based on the Tsyganenko 1989 magnetosphere model, J. Geomag. Geoelectr., 44, 1145–1158, 1992.